Characterization of an F-actin-binding Domain in the Cytoskeletal Protein Vinculin

Annette R. Menkel,*‡ Martina Kroemker,*‡ Peter Bubeck,*‡ Melanie Ronsiek,* Gerd Nikolai,*§ and Brigitte M. Jockusch*‡

*Cell Biology Group, University of Bielefeld, D-33501 Bielefeld, Germany; ‡Cell Biology, Zoological Institute, Technical University of Braunschweig, D-38092 Braunschweig, Germany; and §Institute for Immunology, University of Witten-Herdecke, D-58448 Witten, Germany

Abstract. Vinculin, a major structural component of vertebrate cell–cell and cell–matrix adherens junctions, has been found to interact with several other junctional components. In this report, we have identified and characterized a binding site for filamentous actin. These results included studies with gizzard vinculin, its proteolytic head and tail fragments, and recombinant proteins containing various gizzard vinculin sequences fused to the maltose binding protein (MBP) of *Escherichia coli.*

In cosedimentation assays, only the vinculin tail sequence mediated a direct interaction with actin filaments. The binding was saturable, with a dissociation constant value in the micromolar range. Experiments with deletion clones localized the actin-binding domain to a region confined by residues 893–1016 in the 170-residue-long carboxyterminal segment, while the proline-rich hinge connecting the globular head to the rodlike tail was not required for this interaction.

In fixed and permeabilized cells (cell models), as well as after microinjection, proteins containing the actin-binding domain specifically decorated stress fibers and the cortical network of fibroblasts and epithelial cells, as well as of brush border type microvilli. These results corroborated the sedimentation experiments.

Our data support and extend previous work showing that vinculin binds directly to actin filaments. They are consistent with a model suggesting that in adhesive cells, the NH_2-terminal head piece of vinculin directs this molecule to the focal contact sites, while its tail segment causes bundling of the actin filament ends into the characteristic spear tip–shaped structures.

VINCULIN is an important component of junctional complexes. Its 116-kD polypeptide chain, folded into a large NH_2-terminal head and an extended rodlike tail (7, 8, 24, 25) was localized at the cytoplasmic face of both, cell–matrix and cell–cell junctions in vertebrates and invertebrates. It is indispensible for correct cell attachment and mobility, as shown by several independent lines of evidence. Focal adhesions of cultured fibroblasts are effectively disrupted upon microinjection of monoclonal antibodies directed against several epitopes in the vinculin head (34), and interference with the correct level of vinculin expression leads to drastic alterations in cellular morphology, adhesiveness and motility (10–12). Mutations in the single vinculin gene are incompatible with normal development in the nematode (2). In vitro, the protein, as isolated from chicken smooth muscle, interacts with several other junctional components, i.e., talin, α-actinin, paxillin, tensin, and with itself, and also with acidic phospholipids (see references 14, 16, 23, 26, and 27). While talin, α-actinin and tensin are all believed to bind to actin as well, for vinculin, the corresponding experimental data (17–19, 29, 34) have been controversely discussed (26, 35, 36). In particular, the purity of vinculin preparations used to show binding to filamentous actin was questioned, and contaminating proteins were suggested as mediators for such interactions.

To define more precisely the putative actin binding of vinculin, we have expressed part of its sequence as a fusion protein in *Escherichia coli* and analyzed the interaction of the recombinant protein and of two deletion clones with actin filaments in cosedimentation assays, in cell models and in living cells. Comparative studies were performed with gizzard vinculin and its head and tail fragments. Our data show that the tail segment binds to filamentous actin. The specificity of this reaction is delineated by a 123-amino acid–long stretch in the center of the tail sequence.

Together with previous data on vinculin–vinculin (24, 25) and vinculin–talin (21) interactions, these data contribute to our knowledge on how actin filaments may be organized at the membrane-attachment site of adhesive cells.

Address all correspondence to B. M. Jockusch, Cell Biology, Zoological Institute Biocenter, Technical University of Braunschweig, D-38092 Braunschweig, FRG. Tel.: (49) 531 391 3183. Fax: (49) 531 391 8203.

Materials and Methods

Generation of the vinculin cDNA clones. Total RNA was isolated from turkey gizzard, using the method of Chirgwin et al. (6), and analyzed by electrophoresis in 1% agarose under denaturing conditions (13). cDNA synthesis was performed with RNAse H^--reverse transcriptase (200 U/μl, in 1× RT buffer; Life Technologies, Eggenstein, Germany), supplemented with 0.25 mM dNTP each, 0.1 M DTT, 5 μg/μl BSA, RNAsin (25 U/μl; Promega Biotec Corp., Madison, WI) in a 20 μl reaction volume, containing 2 μg purified RNA, and 2 μg/ml random primer (Boehringer-Mannheim GmbH, Mannheim, Germany) or 1 μg/μl antisense oligonucleotide, respectively.

The vinculin tail-specific sequence was amplified from this template by PCR. The primers used were based upon base pairs 2668-2691 (24 mer) and base pairs 3425-3449 (25 mer) of the chicken vinculin sequence (28). Amplification was performed with Taq DNA polymerase (Life Technologies) as described (22). The product was subjected to electrophoresis in agarose gels, blotted by alkaline transfer onto Hybond N-membrane (Amersham Buchler, Braunschweig, Germany), and hybridized to a digoxigenin-labeled internal oligonucleotide. Hybridization and digoxigenin detection were as described (Boehringer Application Manual, 1989).

Subsequently, the PCR fragment was cloned blunt end into the vector pUC13, to obtain the pUC13/V3 clone. For amplification of the vinculin insert, a modified sense primer consisting of the 24 mer described above, extended at the 5'end by a HpaI restriction site and an ATG start codon replacing ATC at base pairs 2668-2670, and an M13/pUC reverse sequencing primer were used. The resulting PCR product was digested with HpaI and PstI and cloned into the multiple cloning site of the vector pMAL-c (New England Biolabs, Schwalbach, Germany).

The deletion clones MBPVinc8 Δ1 and Δ2 were obtained as PCR products from pUC13/V3. 27-mer primers were used at 5' and 3' ends. Both mutants were also cloned into the pMal-c2 vector, using XbaI and EcoRI restriction sites.

The clones were sequenced by the dideoxy chain termination technique (30), using the T7 sequencing kit (Pharmacia Biosystems, Freiburg, Germany). The primers used were either the universal and the reverse sequencing primers (Boehringer-Mannheim GmbH), or the malE primer and internal oligonucleotides. The cloned sequence vinc8 (base pairs 2671-3435) contained exclusively nucleotide substitutes in the 3 position of 19 triplets, as compared to the chicken sequence (7). Thus, the amino acid sequences were identical between chicken and turkey vinculin tail sequences, but Vinc8 (residues 809-1063) lacked the last three amino acids as compared to the genuine protein. The deduced amino acid sequences of clones Δ1 and Δ2 extended from residue 893 or 1016 to residue 1066, respectively.

Expression and Purification of MBPVinc8 and the Deletion Mutants

E. coli TB1 (araΔ[lacproAB] rpsL [Φ80 lacZΔM15] hsdR) was transformed with the vector pMAL-c/8 and grown in LB medium containing 150 mg/l ampicillin and 2 g/l glucose. Expression of MBPVinc8 was induced by the addition of 1 mM isopropylthiogalactoside to a log phase culture. After at least 12 h growth, bacteria were harvested by a low-speed spin and resuspended in ice-cold 0.01 M TrisHCl, pH 7.2, supplemented with a protease inhibitor cocktail. They were lysed by the addition of lysozyme (1 mg/ml) and sonication (10 min, 18 microns). Protein concentration of the supernatant obtained by centrifugation (30,000 *g*, 1 h) was determined as described (4) and adjusted to 2.5 mg/ml. Affinity chromatography was performed on amylose resin (New England Biolabs, Beverly, MA), with 10 mM maltose in the elution buffer. When necessary, additional purification was achieved by FPLC (Pharmacia, Uppsala, Sweden) on a MonoQ HR 5/5 anion exchange column in 0.01 TrisHCl, pH 8.0, and a NaCl step gradient (10 mM steps, 0–0.8 M). Both deletion mutants were expressed and purified as described for MBPVinc8, with the exception of using *E. coli* JM 105 (lacI^{q}Δ [lacZ] M15 Δ [lac-proAB]) instead of TB1.

Purification of Additional Proteins and Proteolytic Digestion

The maltose-binding protein (MBP)[1] of *p*-MAL-c–transformed bacteria was purified on maltose resin as described above for MBPVinc8 and its deletion relatives. Actin and vinculin were purified from rabbit skeletal muscle and chicken gizzard, respectively, as described (9, 17, 32). Purity of all protein preparations was controlled by SDS-PAGE (see below). Purified MBPVinc8 and chicken gizzard vinculin were digested with V8 protease from *Staphylococcus aureus* (Sigma, Deisenhofen, Germany), at molar ratios of 1:27 (V8/substrate protein). Digestion was terminated by rapid cooling to 0°C and the addition of protease inhibitor cocktails. The 90-kD head and 29/27-kD tail fragments of gizzard vinculin were separated on DEAE-sepharose equilibrated in 0.02 M Tris-acetate, pH 7.6, 0.02 M NaCl, 15 mM β-mercaptoethanol, 0.1 mM EDTA. The 90-kD fragment bound to the anion exchange resin could be eluted with a linear salt gradient. MBPV was obtained by affinity chromatography on amylose resin. The 29/27-kD fragments and Vinc8 were recovered from the unbound material and concentrated. Alternatively, these fragments were purified by cation exchange chromatography, using CM 52-cellulose and an elution buffer of 0.3 M NaCl.

Gel Electrophoresis and Immunoblotting

Proteins were separated either by SDS-PAGE or tricine-SDS-PAGE (31), on 10% polyacrylamide gels. They were either stained with Coomassie brilliant blue or transferred to nictrocellulose. Immunolabeling was performed with a polyclonal rabbit antibody against MBP (New England Biolabs) or a monoclonal antibody against chicken gizzard vinculin (As2; 34). As2 is chicken specific, its epitope was mapped to the region delineated by both V8-cutting sites (E850 and E857, respectively, see Fig. 2; Nicolai, G., and B. M. Jockusch, unpublished data). In this region, two amino acids present in the chicken sequence (H851 and H853) are substituted in the mammalian sequence (15, 33). Immunolabeling of the deletion mutants MBPVinc8 Δ1 and Δ2 was performed with a rabbit antibody against a COOH-terminal vinculin peptide comprising amino acids 1028–1042. Goat-anti–rabbit IgG or rabbit-anti–mouse IgG, both coupled to horse radish peroxidase (Sigma) in conjunction with chloronaphtol/H_2O_2 were used for immunodetection.

Cosedimentation Assay

F-actin binding of proteins and proteolytic fragments was assessed by airfuge sedimentation. Monomeric (G−) actin (1 mg/ml) was induced to polymerize in 0.01 M imidazol, pH 7.4, 1 mM ATP, 0.1 M KCl, 2 mM $MgCl_2$ (F buffer) at 37°C for 45–60 min. MBPVinc8, the V8-generated fragments MBPV and Vinc8, the deletion mutants MBPVinc8 Δ1 and Δ2, gizzard vinculin, the V8-generated 90 and 29/27-kD fragments, and MBP were all dialyzed into F buffer and incubated with F-actin for additional 45 min at 37°C before centrifugation. Salt dependence of the interaction was tested by supplementing F buffer with increasing concentrations of KCl, up to 1 M. For quantitative assays, increasing concentrations of binding candidates were incubated with a fixed concentration (1.1 μM) of actin. After airfuge centrifugation (100,000 *g*, 45 min), supernatants and pellets (washed once with F buffer) were analyzed by SDS-PAGE. The Coomassie brilliant blue–stained bands were quantified by densitometry (Chromoscan; Joyce-Loebl, Gateshead, UK), or by image scanning with Ricoh/Quantiscan (1991; Biosoft, Cambridge, UK).

Preparation of Cell Models, Microinjection, and Fluorescence Analysis

Mouse (Swiss 3T3) and rat (primary) fibroblasts and LLC-PK1 porcine epithelial cells were grown in DME supplemented with 10–12% fetal calf serum. They were seeded onto coverslips at least 24 h before usage. For binding studies on extracted cell models, mouse cells were fixed with 3.7% formaldehyde for 20 min, permeabilized with 0.2% Triton X-100 for 30 min, and incubated with the various proteins (in at least 4×10^{-6} M concentrations) at room temperature for 30 min. The cells were washed extensively in phosphate-buffered saline before the addition of specific antibodies. These included the monoclonal antibody As8 which recognizes a chicken-specific epitope in the 90-kD head fragment of vinculin (34) for the detection of this fragment and intact gizzard vinculin, and anti-MBP for all fusion proteins. TRITC-labeled goat-anti–mouse IgG (Sigma) was used as a second antibody. The 29/27-kD vinculin tail fragment was directly labeled with TRITC, as no chicken-specific antibody recognizing an epitope in the 27-kD fragment was available. Controls included the use of TRITC-conjugated MBP and antibodies without previous addition of target proteins.

Rat fibroblasts were microinjected with 2 mg/ml MBPVinc8 in phosphate-buffered saline. Injection was performed with glass capillaries as previously described (20). The injected cells were incubated for 2 h before fixation and processing for immunofluorescence as described above. The distribution of injected MBPVinc8 was detected with the monoclonal anti–

1. *Abbreviation used in this paper*: MBP, maltose-binding protein.

vinculin As2 (see above). Purified MBP was injected into control cells, and localized with anti-MBP and Rh-goat-anti-rabbit IgG.

In cell models as well as in microinjected cells, F-actin was counterstained by FITC-phalloidin. All preparations were examined in a Zeiss Axiophot equipped with epifluorescence, and photographed on Kodak Tri-X-Pan.

Results

The carboxyterminal sequence of vinculin binds to F-actin. As reported previously (17, 29), vinculin purified from chicken gizzard sediments with filamentous actin. To identify putative actin-binding regions in vinculin, we probed the actin-binding ability of the two main fragments obtained by proteolytic cleavage with the *Staphylococcus aureus* V8 protease (7). The fragments could be purified on CM 52-cellulose, but the COOH-terminal fragment (~29 kD) was unstable and rapidly degraded into a 27-kD fragment. In a first set of sedimentation assays, it was seen that part of the 29/27 COOH-terminal fragment cosedimented with actin filaments, while the 90-kD NH_2-terminal fragment remained in the supernatant (Fig. 1). To further delineate the putative actin-binding domain, we cloned and expressed three pieces of the vinculin tail as fusion proteins in *E. coli*. Fig. 2 shows schematic views of the three proteins, their relation to gizzard vinculin, and the proteolytic cleavage sites of the V8 protease. All three constructs were purified to homogeneity by affinity chromatography on amylose resin, as seen in Fig. 3. Their identity was confirmed with antibodies against MBP and a vinculin tail peptide, respectively (Fig. 3).

Binding of these recombinant proteins to F-actin was analyzed in sedimentation assays. Fig. 4 shows that the purified fusion protein MBPVinc8 and its cleavage product Vinc8, obtained from V8 digestion, both cosedimented with filamentous actin, while the NH_2-terminal proteolytic fragment, MBPV, as well as MBP purified directly from isopropyl-thiogalactoside-induced bacteria, both remained in the supernatant. These results confirmed the location of an actin-binding domain within the COOH-terminal sequence, which was also active in the recombinant fusion protein and its isolated tail fragment (cf. Fig. 4 with Fig. 1). Furthermore, they showed that when mixed in equimolar ratios with actin, only part of MBPVinc8 sedimented, but all of it could be accounted for in the pelleted and soluble fractions. For Vinc8, the proteolytic fragment, the situation was different. As seen in Fig. 4, it was only found in the pellet after cosedimentation with actin, but the recovery was not quantitative. Thus, part of it was apparently degraded during incubation and sedimentation in F-actin buffer. Therefore, for quantification studies, we preferred to use the intact fusion protein MBPVinc8.

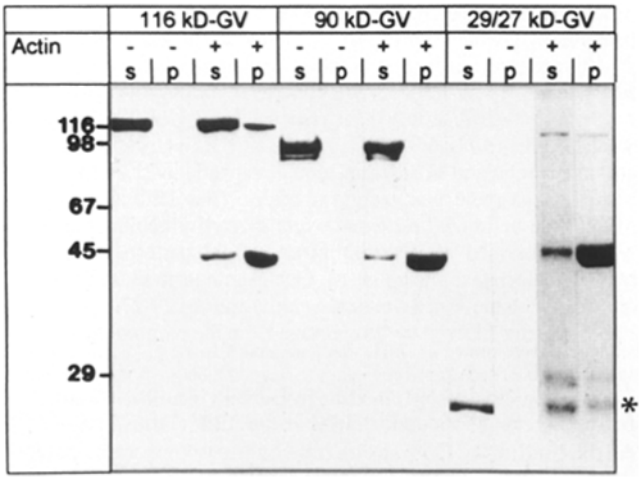

Figure 1. Cosedimentation of vinculin and its V8 protease generated fragments with F-actin. Purified gizzard vinculin (*116 kD-GV*), the large NH_2-terminal (*90 kD-GV*), and the small COOH-terminal (*29/27 kD-GV*) fragments were incubated in F-actin buffer in the presence (+) or absence (−) of skeletal muscle actin and centrifuged in an airfuge. The polypeptide profiles shown were obtained from supernatants (*s*) and pellets (*p*) by SDS-PAGE. Molecular weight markers are given on the left. (*) Position of the 27-kD fragment. The proportion of 29/27-kD fragments varied, indicating that the smaller one is generated by proteolysis from the larger fragment. Partial sedimentation of the intact gizzard protein and of the 29/27 fragments with actin is seen. In contrast, the 90-kD head piece remained quantitatively in the supernatant.

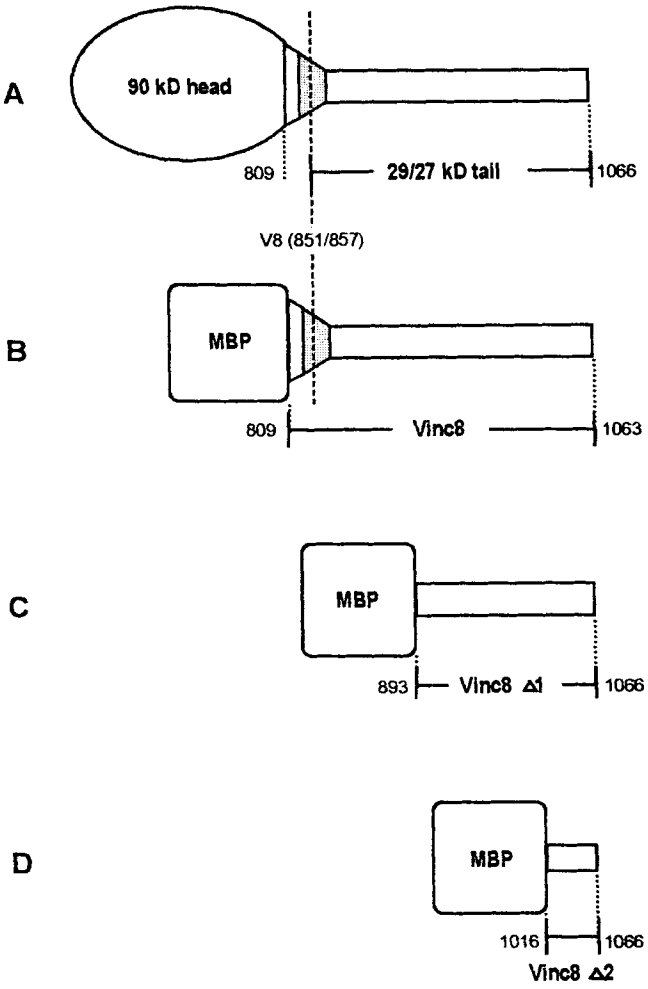

Figure 2. Schematic representation of the gizzard vinculin molecule (*A*) and the recombinant constructs (*B–D*). The proline-rich region is defined by a shaded area, the cleavage sites of the V8 protease (at amino acid positions 851 and 557) within this region are shown. Bold letters indicate the names used for the different fragments. *MBP*, maltose binding protein.

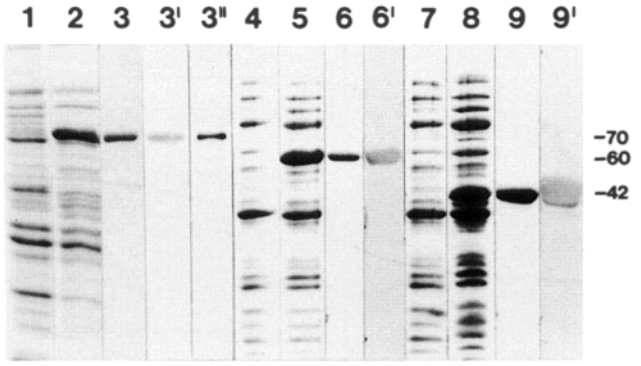

Figure 3. Expression and purification of the recombinant proteins MBPVinc8 and the deletion clones Δ1 and Δ2. Lanes *1*, *4*, and *7* show the soluble polypeptide patterns after separation on SDS gels and Coomassie blue staining of noninduced bacteria for MBPVinc8, clone Δ1 and Δ2, respectively, lanes *2*, *5*, and *8* show the profiles after induction. The purified proteins are shown in lanes *3* (MBPVinc8), *6* (Δ1), and *9* (Δ2). They were identified by immunoblotting with anti-MBP (lane *3'* for MBPVinc8, lane *6'* for Δ1 and lane *9'* for Δ2), and, in the case of MBPVinc8, also with the anti-vinculin As2. Molecular weight markers are given on the right.

Binding of the Vinculin Tail Sequence to Actin Is Saturable and Specific

Quantification of the sedimentable material was used to determine the affinity of MBPVinc8 and of gizzard vinculin for F-actin. Fig. 5 *A* shows the gel analysis of pellets (lanes *1–10*) and supernatants (lanes *1'-10'*) obtained after centrifugation of samples in which a constant F-actin concentration (1.1×10^{-6} M) was incubated with varying concentrations of MBPVinc8 ($0.5–9 \times 10^{-6}$ M). Controls included actin and MBPVinc8 (both at 1.1×10^{-6} M) centrifuged separately. As seen in lanes 9/9' and 10/10' (Fig. 5 *A*), actin sedimented quantitatively, while MBPVinc8, except for a trace, remained in the supernatant. Increasing the concentration of MBPVinc8 up to a molar ratio of 4:1 over actin yielded an increase in sedimentable MBPVinc8 (Fig. 5 *A*, lanes *1/1'–5/5'*), but further addition of the fusion protein did not further increase its sedimentable fraction (lanes *6/6'–8/8'*). As the binding of Coomassie blue by the two proteins considered was comparable (cf. Fig. 5 *A*, lanes *9* and *10'*), densitometry of the stained gel bands for supernatants and pellets was used to determine saturation levels, and affinity between the partners. Fig. 5 *B* shows the resulting binding curve. Saturation was seen at a molar ratio of 1.18:1 (MBPVinc8/actin). These values did not change with the ionic strength of the buffer between 0.1 and 1 M KCl (not shown). The dissociation constant, K_d, is in the micromolar range. The sigmoidal shape of the curve indicated cooperative binding. Treatment of the data according to the Hill equation yielded a Hill coefficient of more than 2. Thus, this binding is saturable, cooperative and of an affinity suggestive of a specific interaction.

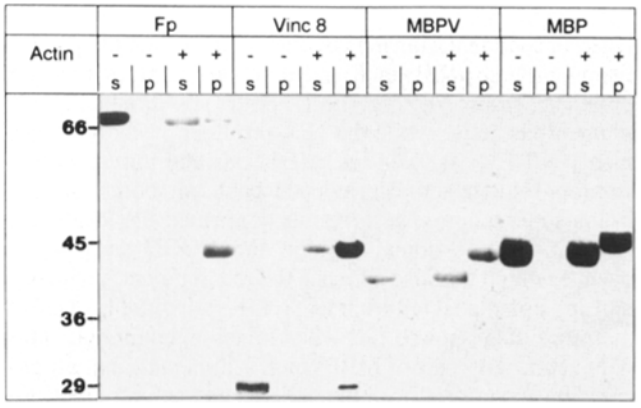

Figure 4. Cosedimentation of recombinant proteins with F-actin. Conditions, gel analysis and molecular weight markers were as described in Fig. 1. The fusion protein MBPVinc8 (*Fp*) cosedimented partially with actin, as did the V8-generated Vinc8 fragment. In contrast, the head fragment of MBPVinc8, MBPV, and the purified maltose-binding protein (*MBP*), both remained quantitatively in the supernatant.

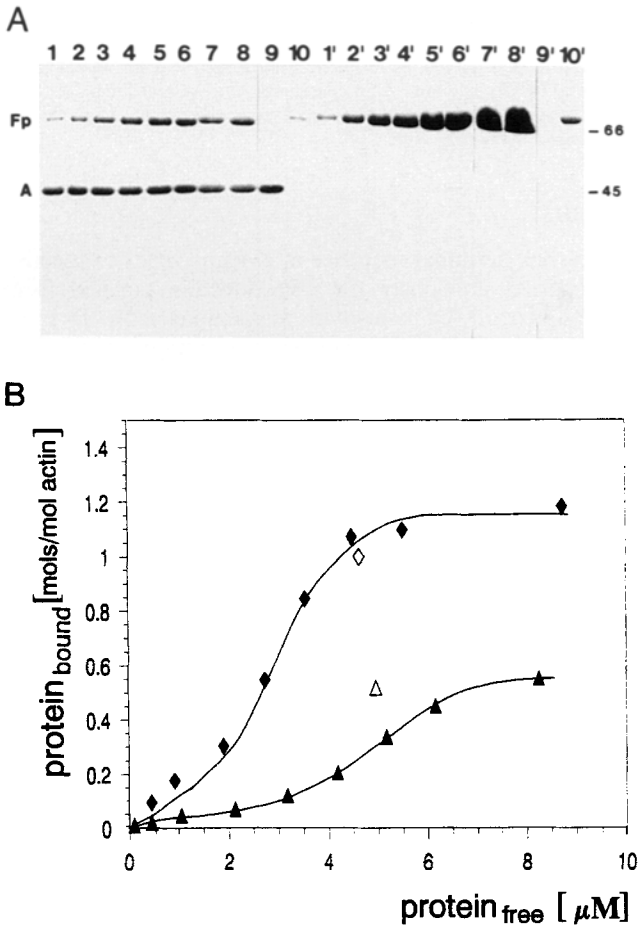

Figure 5. Quantitative analysis of MBPVinc8 and gizzard vinculin binding to actin. (*A*) SDS–polyacrylamide gels showing aliquots of proteins sedimented (lanes *1–10*) or found in the supernatant (lanes *1'–10'*) after centrifugation of the following mixtures: actin (*A*) 1.1 μM in samples *1/1'–9/9'*; MBPVinc8 (*Fp*) in the following molar ratios (MBPVinc8/actin): 0.5:1 (lanes *1/1'*), 1:1 (*2/2'*), 2:1 (*3/3'*), 3:1 (*4/4'*), 5:1 (*6/6'*), 6:1 (*7/7'*), and 9:1 (*8/8'*). Lanes *9/9'* and *10/10'* contained actin and MBPVinc8 alone, respectively (1.1 μM). Numbers refer to molecular weight markers. (*B*) Binding curves for MBPVinc8-actin (*full diamonds*) and gizzard vinculin (*full triangles*) as obtained after densitometry of gel patterns from sedimented material, as shown in (*A*). Open symbols indicate the values obtained with the Vinc8 (*open diamond*) and the 29/27 (*open triangle*) fragments derived by V8 cleavage from the parental molecules.

Analogous experiments were performed with intact gizzard vinculin, to demonstrate the validity of these results for the genuine protein. Fig. 5 *B* reveals that indeed in both cases the binding is saturable and cooperative, as indicated by the sigmoidal shape, and both K_d values were in the micromolar range.

However, the final level of gizzard vinculin binding was below that observed for the fusion protein. To decide whether this was caused by the head portions that differ between these molecules, we repeated the sedimentation assays with the 29/27 kD and Vinc8 fragments, as purified on cation exchange columns from V8 digests. Due to the already mentioned instability of these proteins, this was only performed with selected actin–protein ratios. Fig. 5 *B* demonstrates that the isolated Vinc8 fragment bound to actin with an affinity comparable to that of the intact fusion protein MBPVinc8, while the isolated gizzard tail fragment showed a slightly higher value of F-actin binding as compared to the parental molecule. Thus, in case of the fusion protein, the MBP head did not influence the binding characteristics, while some negative effect was seen by the large NH_2-terminal head of the gizzard protein.

The Actin-binding Domain Involves the Sequence Carboxy-terminal of Amino Acid 893

Binding curves were also obtained for the deletion clones MBPVinc8 Δ1 and Δ2, using again cosedimentation with filamentous actin. Fig. 6 shows that Δ1 also binds to F-actin in a saturable manner, demonstrating that actin binding of the vinculin tail does not depend on the proline-rich sequence which had been deleted from Δ1. Interestingly, this binding curve is not sigmoidal, suggesting that the proline-rich region might confer cooperativity to the actin binding. In case of clone Δ2, which contains only the fifty carboxyterminal residues, the individual measurements scattered substantially. Therefore, the specificity of this reaction was difficult to evaluate, but the overall binding was reduced as compared to Δ1.

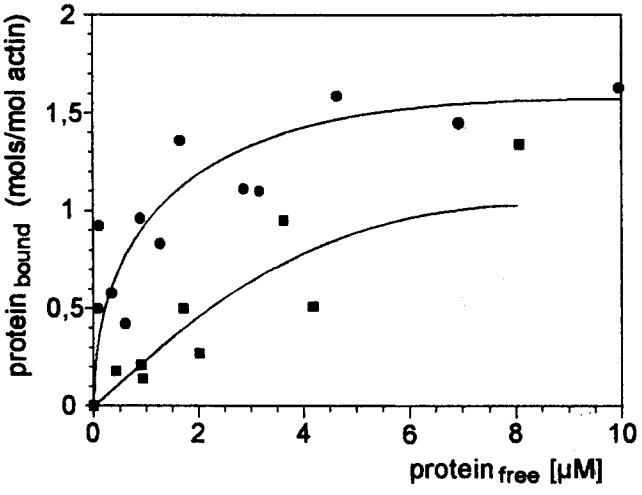

Figure 6. Binding curves obtained with the deletion proteins Δ1 and Δ2. Experimental conditions were as described in Fig. 5. Quantification of the stained gel patterns was achieved by image scanning and computer analysis.

The Vinculin Tail Sequence Binds to the Actin Skeleton in Cell Models

The ability of the vinculin tail sequence to associate with the actin cytoskeleton in cells was tested on fixed and permeabilized cells (cell models). Fig. 7 shows that genuine vinculin preferentially binds to the ends of stress fibers in mouse fibroblasts, as detected with a monoclonal antibody specific for an epitope in the NH_2-terminal region of chicken vinculin (*a*/*a*′–*b*/*b*′). Similar results had previously been obtained with rhodamine-labeled vinculin and L6 cells (1). When cell models were incubated solely with the purified 90-kD head fragment, binding was again seen preferentially at the ends of stress fibers, as detected with the same antibody (Fig. 7, *c*/*c*′ and *d*/*d*′). In contrast, the isolated gizzard 29/27-kD tail fragment, directly labeled with TRITC, decorated the stress fibers homogeneously (Fig. 7 *e*/*e*′). Control cells that had been incubated with antibodies only, or with TRITC-labeled MBP, showed no labeling (not shown). In analogous experiments, the recombinant fusion protein MBPVinc8 and the deletion product Δ1 both bound also alongside stress fibers (Fig. 8, *a*/*a*′ and *b*/*b*′, respectively). Thus, for gizzard vinculin and its proteolytic fragments, and for MBPVinc8 and Δ1, these results matched those obtained in the cosedimentation experiments with pure F-actin. In contrast, no specific stress fiber decoration could be seen with deletion clone Δ2 (Fig. 8 *c*/*c*′). In this case, the results obtained in both assays were not identical, but the reduction in F-actin binding and the absence of specific stress fiber staining are at least not contradictory.

To probe whether stress fiber binding was due to a direct interaction with filamentous actin or mediated by other microfilament proteins, possibly α-actinin, we incubated cell models obtained from the LLC-PK1 cell line with the various vinculin fragments and constructs. Decoration of stress fibers and peripheral belts, superimposable with actin staining, was again seen (not shown). In addition, the brush border type microvilli on the apical surface of these kidney epithelial cells were brightly labeled, as seen in Fig. 8 *d*/*d*′ for the deletion clone Δ1. In contrast, binding of clone Δ2 to these cellular projections was very weak (Fig. 8 *e*/*e*′). As the microvilli of LLC-PK1 cells, like all brush border microvilli, lack α-actinin (Temm-Grove, C., and B. M. Jockusch, unpublished data), this result suggests that the vinculin tail segment binds also directly to actin filaments in cytoskeletal preparations.

The Recombinant Vinculin Tail Sequence Decorates the Actin Skeleton in Living Cells

The ability of the recombinant vinculin tail to interact with microfilaments was also tested in living cells. MBPVinc8 was microinjected into stationary rat fibroblasts and again localized by immunofluorescence with a monoclonal antibody specific for a chicken vinculin epitope (As2). The actin network in these cells was again revealed by double staining with phalloidin. At the needle concentration used (2 mg/ml), the injected recombinant protein did not perturb the prominent stress fiber system developed in these cells, nor did it interfere with cellular adhesion (not shown). However, it decorated the stress fibers in stationary cells along their entire length (Fig. 9, *a*/*a*′ and *c*/*c*′), including their distal portions terminating in focal adhesion sites (Fig. 9, *b*/*b*′). In

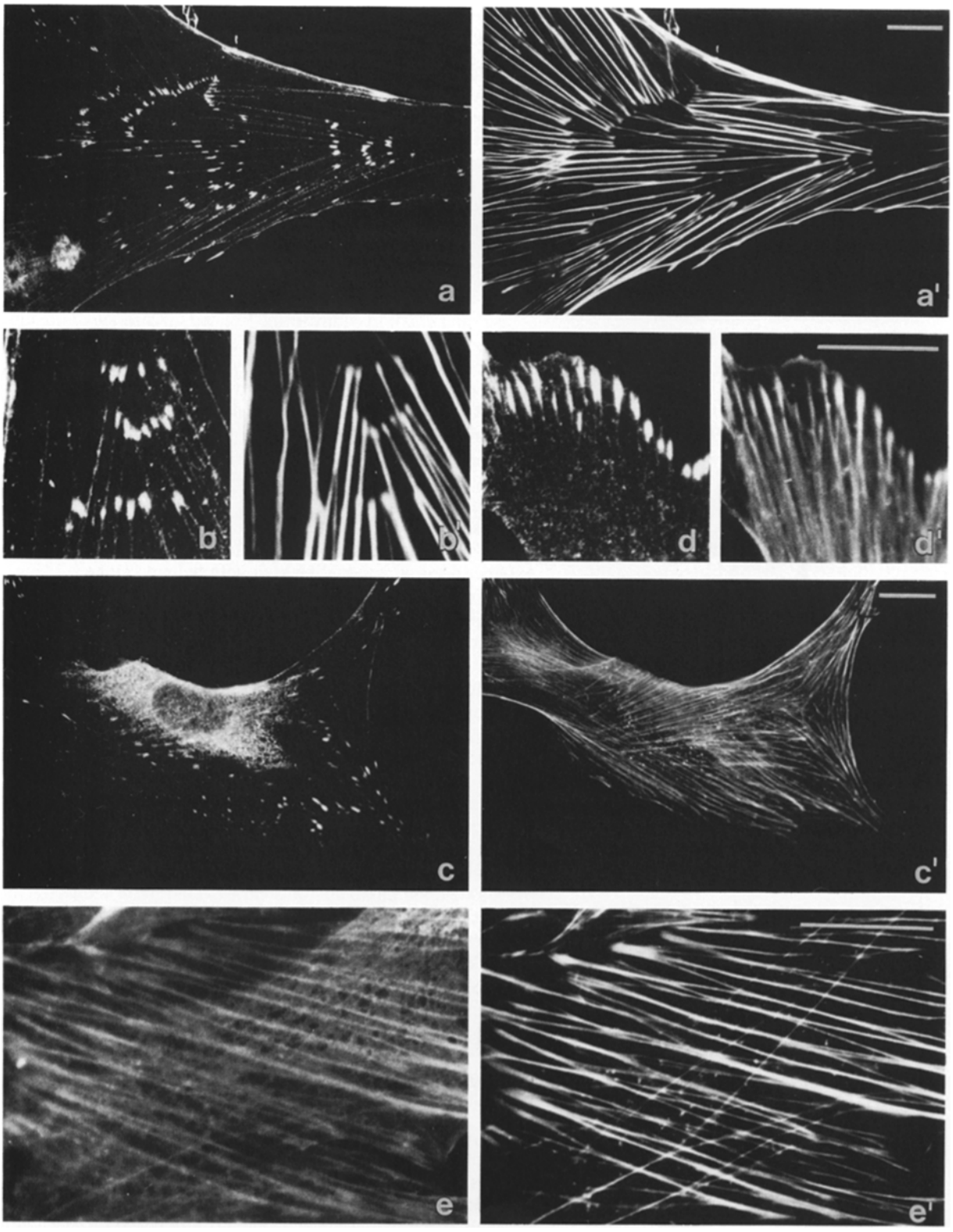

Figure 7. Binding of gizzard vinculin and its fragments to the actin cytoskeleton in mouse fibroblast cell models, as revealed in double fluorescence studies. (*a'–e'*) Actin filament organization as seen after staining with FITC-phalloidin. Binding of intact vinculin (*a* and *b*) and of its 90-kD head portion (*c* and *d*) were revealed by a chicken-specific anti-vinculin (As8) and a TRITC-coupled second antibody. For binding studies with the 29/27-kD tail fragment (*e*), this was directly coupled to TRITC. While the parental gizzard vinculin and the head fragment were preferentially targeted to the focal adhesion sites, the tail fragment decorates actin filament bundles homogeneously. Bars, 20 μm.

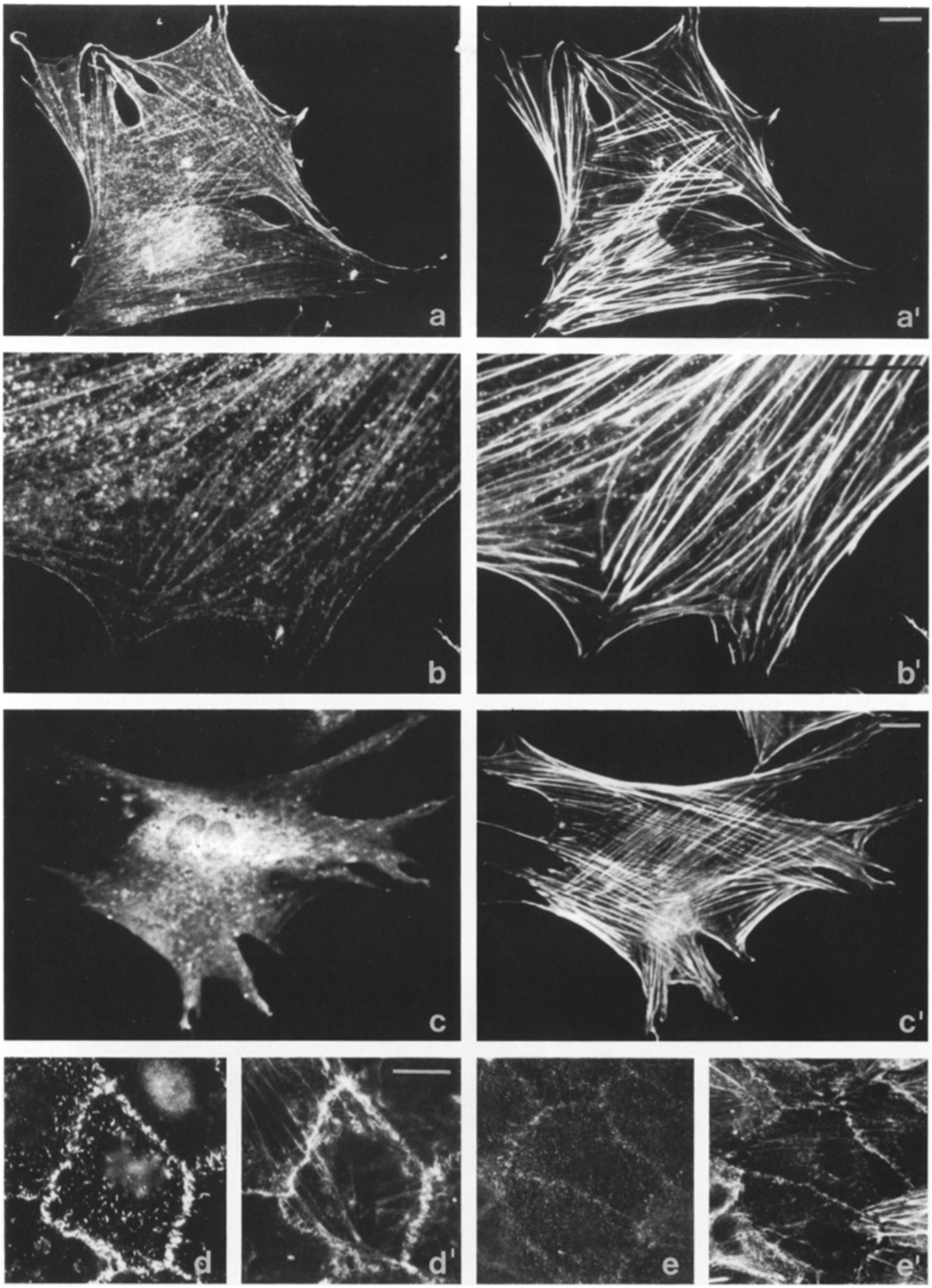

Figure 8. Binding of recombinant proteins to mouse fibroblast and epithelial cell models, as revealed in double fluorescence studies. (*a'–e'*) The actin cytoskeleton as seen after FITC-phalloidin staining; (*a–e*) localization of all constructs as seen with anti-MBP and a second, TRITC-coupled antibody. (*a–c*) Mouse fibroblasts; (*d–e*) LLC-PK1 epithelial cells. (*a*) MBPVinc8; (*b* and *d*) the deletion protein Δ1; (*c* and *e*) the deletion protein Δ2. While MBPVinc8 and Δ1 decorated the stress fiber system in fibroblasts, Δ2 showed no specific binding (cf. *a* and *b* with *c*). Similarly, Δ1 bound specifically to the apical microvilli in the brush border–derived LLC-PK1 cells, but Δ2 showed only a very weak binding (cf. *d* with *e*). Bars: (*a–c'*) 20 μm; (*d'* and *e'*) 10 μm.

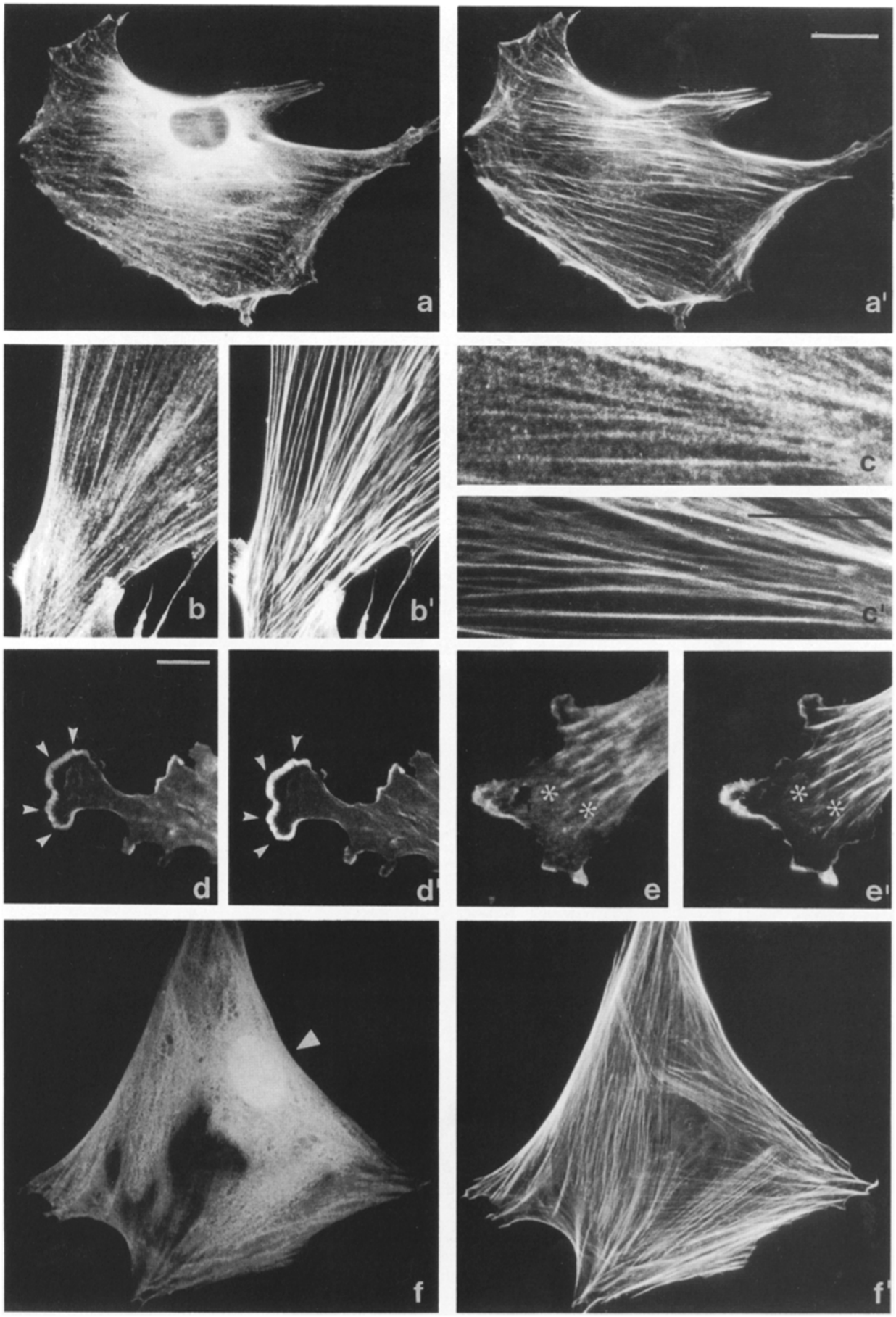
a
a'
b
b'
c
c'
d
d'
e
e'
f
f'

spreading and locomoting cells, the injected protein colocalized with the cortical actin network of lamellipodia (Fig. 9 *d*/*d'*), and with the nascent short microfilament bundles and their characteristic splayed ends frequently found in the rear part of lamellipodia (Fig. 9 *e*/*e'*). Control cells, which were injected with purified MBP showed no such decoration of their actin skeleton, when immunostained with the antibody against MBP, but demonstrated a weak labeling of ill defined structures, and a strong nuclear fluorescence (Fig. 9 *f*/*f'*). Thus, the images seen after microinjecting MBPVinc8 confirmed the results obtained with cell models.

Discussion

In this study, we have probed the interaction of vinculin with actin filaments. Our results demonstrate that the vinculin tail associates with F-actin in sedimentation assays and with cytoskeletal microfilaments in detergent-extracted and living cells. We found good qualitative correspondence between the results obtained with these different approaches.

Binding of gizzard vinculin to skeletal muscle actin has been previously analyzed in sedimentation assays by Ruhnau and Wegner (29). These authors concluded that no more than 1 mole vinculin binds per 100 mol of actin. The data reported in the present study exceed this value by a factor of 50 (0.5 mol of vinculin per mole of actin). These discrepancies may be explained by experimental differences and the fact that these authors did not extend their measurements to higher vinculin/actin ratios and thus may not have reached saturation (Wegner, A., personal communication).

A comparison of genuine and recombinant proteins showed no substantial difference in actin binding and the same was true for proteolytic fragments. Thus, the overall structure of the tail segments obtained by the various techniques was probably similar to that of the parental protein. As there is no information on folding of the amino acid sequence within the rodlike tail, we cannot correlate the identification of an actin-binding domain delineated by amino acid residues 893 and 1063 with a physically defined region in the tail. Likewise, the nature of the interaction with actin remains unknown. Within the basic (pH 9.7; 7) tail sequence, the actin-binding domain is particularly rich in positively charged amino acids, and, therefore, one might have suspected charge interactions to play an important role in binding to the negatively charged actin molecule. However, the complex between MBPVinc8 and F-actin was stable up to 1 M KCl, which argues against a sole ionic interaction.

The biological relevance of the actin binding by vinculin is suggested by the experiments with cell models and the microinjection analyses. We confirmed previous reports (5, 1) on the preferential targeting of the intact protein to the large focal adhesion sites developed in stationary fibroblasts, and found that the same was true for the isolated 90 kD head piece. As this fragment contains a well-defined binding site for talin, another component of focal adhesions (21), these data suggest that vinculin is directed towards this region by the affinity of its head piece for talin.

On the other hand, paxillin, a minor component of focal adhesion sites, has been shown to interact in vitro with a domain comprising residues 978–1000 in the vinculin tail piece, and COS cells and mouse fibroblasts, when transfected with cDNAs containing residues 1000–1028, collect the resulting polypeptides in focal adhesion areas (37). These data support a previous notion on a second adhesion targeting site, located in the vinculin tail (3), in addition to the talin-binding domain in the head. As the experimental design and the constructs used differ from our approach, and no information on folding of the various constructs is available, a direct comparison with our results seems difficult. Competition between paxillin and actin binding, a regulation of the actin binding by paxillin, or additive effects at the focal adhesion sites may all be envisioned.

All data available until now are consistent with the view that cellular vinculin is concentrated in the focal adhesion site by its affinity for talin, and possibly paxillin. There, its high concentration should allow for cluster formation, due to self-aggregation of heads and tails. In such oligomeric clusters, the tails would point away from the plasma membrane. Our data provide evidence that these segments can then interact directly with the terminal portions of actin filaments, thus collecting them into the spear tip–shaped focal contact, and anchoring them in this specific structure at the cytoplasmic face of the plasma membrane.

We thank Dr. H. Faulstich (Heidelberg, FRG) for FITC-phalloidin, Drs. H. Jockusch, H. Hinssen (Bielefeld, FRG), K. Schlüter, K. Giehl, and M. Rothkegel (Braunschweig, FRG) for stimulating discussions, and A. Wegner for permission to quote his personal communication. M. A. Eppe (Bielefeld, FRG) was involved in preliminary experiments of defining the actin-binding fragment in gizzard vinculin.

This work was supported by the Deutsche Forschungsgemeinschaft.

Received for publication 30 March 1994, and in revised form 18 May 1994.

References

1. Ball, E. H., Ch. Freitag, and S. Gurofsky. 1986. Vinculin interaction with permeabilized cells: disruption and reconstitution of a binding site. *J. Cell Biol.* 103:641–648.
2. Barstead, R. J., and R. H. Waterston. 1991. Vinculin is essential for muscle function in the nematode. *J. Cell Biol.* 114:715–724.
3. Bendori, R., D. Salomon, and B. Geiger. 1989. Identification of two distinct functional domains on vinculin involved in its association with focal contacts. *J. Cell Biol.* 108:2383–2393.
4. Bradford, M. M. 1976. A rapid and sensitive method for the quantitation of microgram quantities of protein utilizing the principle of protein–dye binding. *Anal. Biochem.* 72:248–254.
5. Burridge, K., and J. Feramisco. 1980. Microinjection and localization of a 130 K protein in living fibroblasts: a relationship to actin and fibronec-

Figure 9. Fluorescence patterns of rat fibroblasts microinjected with MBPVinc8 or MBP. (*a'-f*) F-actin distribution as seen with FITC-phalloidin. (*a–e*) MBPVinc8 distribution, as revealed after staining with the chicken-specific monoclonal anti-vinculin (As2). (*f*) Localization of MBP as seen with anti-MBP. TRITC-coupled second antibodies were used for detection of the specific antibody in both cases. In stationary cells, MBPVinc8 was targeted to the stress fibers at their entire length, including their terminal portions (*a–c*). In lamellipodia of spreading and locomoting cells, the cortical actin network (*d*, *small arrowheads*) and the ends of nascent microfilament bundles (*e*, *) were decorated by MBPVinc8. In contrast, MBP showed no preference for F-actin in injected cells but labeled the nucleus quite strongly (*f*, arrowhead). Bars: (*a'*, *a*, *b*, and *f*) 20 μm; (*c'*) 20 μm; (*d* and *e*) 5 μm.

tin. *Cell.* 19:587–595.
6. Chirgwin, J. M., A. E. Przybla, R. J. McDonald, and W. J. Rutter. 1979. Isolation of biologically active ribonucleic acid from sources enriched in ribonuclease. *Biochemistry.* 18:5294–5299.
7. Coutu, M. D., and S. W. Craig. 1988. cDNA-derived sequence of chicken embryo vinculin. *Proc. Natl. Acad. Sci. USA.* 85:8535–8539.
8. Eimer, W., M. Niermann, M. A. Eppe, and B. M. Jockusch. 1993. Molecular shape of vinculin in aqueous solution. *J. Mol. Biol.* 229:146–152.
9. Feramisco, J. R., and K. Burridge. 1980. A rapid purification of α-actinin, and a 130,000-dalton protein from smooth muscle. *J. Biol. Chem.* 255:1194–1199.
10. Fernández, J. L. R., B. Geiger, D. Salomon, and A. Ben-Ze'ev. 1992. Overexpression of vinculin suppresses cell motility in BALB/c 3T3 cells. *Cell Motil. Cytoskeleton.* 22:127–134.
11. Fernández, J. L. R., B. Geiger, D. Salomon, and A. Ben-Ze'ev. 1993. Suppression of vinculin expression by antisense transfection confers changes in cell morphology, motility, and anchorage-dependent growth of 3T3 cells. *J. Cell Biol.* 122:1285–1294.
12. Fernández, J. L. R., B. Geiger, D. Salomon, I. Sabanay, M. Zöller, and A. Ben-Ze'ev. 1992. Suppression of tumorgenicity in transformed cells after transfection with vinculin cDNA. *J. Cell Biol.* 119:427–438.
13. Fourney, R. M., J. Miyakoshi, R. S. Day, and M. C. Paterson. 1988. Northern blotting: efficient RNA staining and transfer. *Focus (Life Technologies).* 10:5–7.
14. Geiger, B., and D. Ginsberg. 1991. The cytosplasmic domain of adherens-type junctions. *Cell Motil. Cytoskeleton.* 20:1–6.
15. Gimona, M., J. V. Small, M. Moeremans, J. Van Damme, M. Puype, and J. Vandekerckhove. 1988. Porcine vinculin and metavinculin differ by a 68-residue insert located close to the carboxy-terminal part of the molecule. *EMBO (Eur. Mol. Biol. Organ.) J.* 7:2329–2334.
16. Isenberg, G. 1991. Actin-binding protein-lipid interactions. *J. Muscle Res. Cell Motil.* 12:136–144.
17. Isenberg, G., K. Leonard, and B. M. Jockusch. 1982. Structural aspects of vinculin-actin interactions. *J. Mol. Biol.* 158:231–249.
18. Jockusch, B. M., and G. Isenberg. 1981. Interaction of α-actinin and vinculin with actin: Opposite effects on filament network formation. *Proc. Natl. Acad. Sci. USA.* 78:3005–3009.
19. Jockusch, B. M., and G. Isenberg. 1982. Vinculin and α-actinin interaction with actin and effect on microfilament network formation. *Cold Spring Harbor Symp. Quant. Biol.* 46:613–623.
20. Jockusch, B. M., B. Zurek, R. Zahn, A. Westmeyer, and A. Füchtbauer. 1992. Antibodies against vertebrate microfilament proteins in the analysis of cellular motility and adhesion. *J. Cell Sci. Suppl.* 14:41–47.
21. Jones, P., P. Jackson, G. J. Price, B. Patel, V. Ohanion, A. L. Lear, and D. R. Critchley. 1989. Identification of a talin-binding site in the cytoskeletal protein vinculin. *J. Cell Biol.* 109:2917–2927.
22. Linz, U., U. Dellin, and H. Rübsamen-Waigmann. 1990. Systematic studies on parameters influencing the performance of the polymerase chain reaction. *J. Clin. Chem. Clin. Biochem.* 28:5–13.
23. Luna, E. J., and A. L. Hitt. 1992. Cytoskeleton-plasma membrane interactions. *Science (Wash. DC).* 258:955–964.
24. Milam, L. M. 1985. Electron microscopy of rotary shadowed vinculin and vinculin complexes. *J. Mol. Biol.* 184:543–545.
25. Molony, L., and K. Burridge. 1985. Molecular shape and self-association of vinculin and metavinculin. *J. Cell Biochem.* 29:31–36.
26. Otto, J. J. 1986. The lack of interaction between vinculin and actin. *Cell Motil. Cytoskel.* 6:48–55.
27. Otto, J. J. 1990. Vinculin. *Cell Motil. Cytoskeleton.* 16:1–6.
28. Price, G. L., P. Jones, M. D. Davison, B. Patel, R. Bendori, B. Geiger, and D. R. Critchley. 1989. Isolation and characterization of a vinculin cDNA from chick-embryo fibroblasts. *Biochem. J.* 259:453–461.
29. Ruhnau, K., and A. Wegner. 1988. Evidence for direct binding of vinculin to actin filaments. *FEBS (Fed. Eur. Biochem. Soc.) Lett.* 228:105–108.
30. Sanger, F., S. Nicklen, and A. R. Coulson. 1977. DNA sequencing with chain terminating inhibitors. *Proc. Natl. Acad. Sci. USA.* 74:5463–5467.
31. Schägger, H., and G. von Jagow. 1987. Tricine-sodium dodecyl sulfate-polyacrylamide gel electrophoresis for the separation of proteins in the range from 1–100 kda. *Anal. Biochem.* 166:368–379.
32. Spudich, J. A., and S. Watt. 1971. The regulation of rabbit skeletal muscle contraction. I. Biochemical studies of the interaction of the tropomyosin–troponin complex with actin and the proteolytic fragments of myosin. *J. Biol. Chem.* 246:4866–4871.
33. Weller, P. A., E. P. Ogryzko, E. B. Corben, N. I. Zhidkova, B. Patel, G. J. Price, N. K. Spurr, V. E. Koteliansky, and D. R. Critchley. 1990. Complete sequence of human vinculin and assignment of the gene to chromosome 10. *Proc. Natl. Acad. Sci. USA.* 87:5667–5671.
34. Westmeyer, A., K. Ruhnau, A. Wegner, and B. M. Jockusch. 1990. Antibody mapping of functional domains in vinculin. *EMBO (Eur. Mol. Biol. Organ.) J.* 9:2071–2078.
35. Wilkins, J. A., and S. Lin. 1982. High affinity interactions of vinculin with actin filaments *in vitro*. *Cell.* 28:83–90.
36. Wilkins, J. A., and S. Lin. 1986. A reexamination of the interaction of vinculin with actin. *J. Cell Biol.* 102:1085–1092.
37. Wood, C. K., C. E. Turner, P. Jackson, and D. R. Critchley. 1994. Characterisation of the paxillin-binding site and the C-terminal focal adhesion targeting sequence in vinculin. *J. Cell Sci.* 107:709–717.